Colloids and Surfaces B: Biointerfaces 255 (2025) 114929

Contents lists available at ScienceDirect

Colloids and Surfaces B: Biointerfaces

journal homepage: www.elsevier.com/locate/colsurfb

Synergistic effects of borneol and zwitterionic coating on enhanced antimicrobial and anti-biofilm performance

Chen Chen [a], Songtao Wang [a], Wenjing Niu [a], Fang Liu [c], Wensheng Xie [a], Guofeng Li [a,*], Dongsheng Kong [b,*], Xing Wang [a,*]

[a] State Key Laboratory of Organic-Inorganic Composites, Beijing Laboratory of Biomedical Materials, College of Life Science and Technology, Beijing University of Chemical Technology, Beijing 100029, PR China
[b] Department of Neurosurgery, First Medical Center, PLA General Hospital, Beijing 100853, PR China
[c] Department of Oncology of Integrative Chinese and Western Medicine, China-Japan Friendship Hospital, Beijing 100029, PR China

ARTICLE INFO

Keywords:
Zwitterions
Borneol
Antimicrobial adhesion
Anti-biofilm
Coating

ABSTRACT

Infections caused by microorganisms on the surfaces of medical implants and devices represent a significant challenge in the field of medicine. At present, a considerable number of antimicrobial coatings have been developed with the objective of preventing bacterial contamination. However, the problem of mold contamination is often underestimated. To address this issue, a bi-molecular composite coating was developed using sulfobetaine and borneol unites, which enabled the modification of polydimethylsiloxane (PDMS) substrates. Furthermore, by modifying the ratio of sulfobetaine and borneol groups, the coating can simultaneously demonstrate anti-bacterial, anti-mold adhesion and anti-biofilm properties. Notably, the bi-molecular polymer coating exhibited a synergistic effect in inhibiting bacterial biofilm formation. Subsequent *in vivo* subcutaneous implantation in mice confirmed its favorable biocompatibility. Therefore, this approach offers novel insights into the development of antimicrobial adhesion coatings for medical device surfaces, particularly those need to prevent biofilm formation.

1. Introduction

Microbial infections are a significant cause of mortality in the healthcare field [1]. Among them, pathogenic microorganisms adhere to the surface of materials and form biofilms that are difficult to remove [2]. These biofilms not only contribute to persistent infections but can also lead to severe complications or even death. It is estimated that about 80 % of human infections are associated with biofilms [3]. Furthermore, the long-term use of high-dose antibiotics has contributed to microbial resistance, which is a significant challenge for clinical treatment [4]. Therefore, imparting antimicrobial properties to material surfaces is urgently needed to limit the spread of microorganisms and reduce the risk of infection.

Various antimicrobial surface coatings have been designed to resist bacterial contamination, such as quaternary ammonium salts, metal ions, and antimicrobial peptides [5–7]. These strategies demonstrate considerable potential for enhancing the antimicrobial properties of substrates. However, most of these coatings primarily rely on bactericidal mechanisms, particularly those involving the release of active agents, which may raise environmental and biocompatibility concerns during long-term use [8,9]. Furthermore, their antibacterial efficacy may gradually decline due to the accumulation of bacterial debris on the surface, which can cover the active functional groups of the coating and lead to subsequent microbial adhesion [10]. These limitations are especially critical in the biofilm formation, as once initial microbial adhesion occurs, it can readily progress into mature and persistent biofilms on material surfaces. Biofilms are primarily composed of microorganisms embedded in a matrix of extracellular polymeric substances (EPS), including eDNA, polysaccharides, lipids, and proteins [11]. Compared with their planktonic counterparts, microbes within biofilms exhibit markedly enhanced resistance to antimicrobial agents and environmental stressors. Once established, biofilms are exceptionally difficult to eradicate and can effectively evade host immune defenses [12].

In recent years, hydrophilic antimicrobial adhesion surfaces, represented by zwitterionic materials, have drawn increasing attention. They are considered promising alternatives to polyethylene glycol for antifouling applications, offering significant advantages in terms of

* Corresponding authors.
E-mail addresses: ligf@mail.buct.edu.cn (G. Li), kongdongsheng@301hospital.com.cn (D. Kong), wangxing@mail.buct.edu.cn (X. Wang).

https://doi.org/10.1016/j.colsurfb.2025.114929
Received 15 May 2025; Received in revised form 25 June 2025; Accepted 1 July 2025
Available online 2 July 2025
0927-7765/© 2025 Published by Elsevier B.V.

biocompatibility [13,14]. Notably, zwitterionic coatings effectively resist nonspecific protein adsorption and bacterial adhesion, thereby inhibiting early biofilm formation. However, the research mainly focuses on the design of anti-bacteria, while mold contamination is often ignored. As filamentous fungi (e.g., molds) are known to exhibit a preference for moist environments, hydrophilic or anti-adhesive strategies that effectively inhibit bacterial adhesion may not be equally effective against fungal colonization [15,16]. This highlights the need for targeted and broad-spectrum antimicrobial surface design. In addition, it is reported that about 10 million people are at risk of *Aspergillus* diseases in world, particularly those with weakened immune systems [17]. Even with diagnosis and treatment, the overall mortality rate of invasive aspergillosis remains exceedingly high (over 50 %) [18]. Therefore, the anti-mold adhesion performance of the material warrants further investigation.

The recent development of stereochemical antimicrobial approaches has introduced innovative insights into antimicrobial research [19]. Studies have shown that terpenoid molecules with stereochemical structures, predominantly natural compounds such as borneol and menthol, when present on the surface of materials, can effectively inhibit the adhesion of bacteria and mold [20–22]. Their potential for application in the field of antimicrobial agents is considerable.

Based on these insights, this study systematically investigated the effects of different ratios of sulfobetaine and borneol units on the antimicrobial adhesion properties of bacteria and mold. Using thiol-ene click chemistry, we created bi-molecular composite coatings with PDMS as the substrate, which is the most common material in the medical field. The antimicrobial adhesion and anti-biofilm properties of bi-molecular polymer coatings with varying sulfobetaine methacrylate and isobornyl acrylate (SBMA/BA) ratios were investigated, highlighting their potential for preventing microbial infection.

2. Materials and methods

2.1. Experimental materials

Isobornyl acrylate (BA, 99 %) was obtained from RYOJI Chemical Co., Ltd., Sulfobetaine methacrylate (SBMA, 98 %) and 2,2-bimethoxy-2-phenylacetophenone (DMPA, 99 %) were obtained from Shanghai yuanye Bio-Technology Co., Ltd. Trimethylolpropane triacrylate (TMPTA, 98 %) was purchased from Dongguan Sanhe Plastics Co., Ltd. Methanol and dichloromethane were purchased from Damao Chemical Plant (Tianjin). The PDMS (Sylgard 184) was obtained from Songsen New Materials Technology Co., Ltd (Shenzhen). γ-Mercaptopropyltrimethoxysilane (MTS) was obtained from J&K Scientific. Potassium hydroxide was purchased from Beijing Chemical Work (KOH, 99 %). *Escherichia coli* (*E. coli*, ATCC 25922), *Staphylococcus aureus* (*S. aureus*, ATCC 25923) and *Aspergillus niger* (*A. niger*, CICC 41254) were obtained from the China General Microbiological Culture Collection Center. Malt extract agar, Tryptone soy agar (TSA) and trypticase soy broth (TSB) medium were purchased from Aoboxing Biotechnology Co., Ltd. The L929 mouse fibroblast cells were obtained from the Cell Resource Center of the Chinese Academy of Medical Sciences and Peking Union Medical College (Beijing). The Calcein AM/PI double stain kit and thiazolyl blue tetrazolium bromide (MTT) were purchased from Solarbio Science & Technology Co., Ltd. (China). Sodium dodecyl sulfate (SDS, 98 %) was supplied by Aladdin Ltd., (Shanghai, China). Female BALB/c mice, 5 weeks old (~16g), were obtained from Vital River Laboratory Animal Technology Co., Ltd.

2.2. Preparation of coatings grafting to PDMS with different ratios of SBMA/BA

The surface of PDMS modified with thiol groups was followed a previously established method [23]. In brief, the cured PDMS was immersed in a methanol solution containing 10 % (v/v) MTS and 1 % (w/v) KOH, then sonicated at 50 °C for 6 h. Afterward, the PDMS was cleaned three times with fresh dichloromethane, with each clean stirring for 3 h. The thiol-modified PDMS (PDMS-SH) was then stored in a methanol solution at 4 °C. Surface grafting process was performed using different molar ratios of BA and SBMA to create polymer coatings. BA, SBMA, TMPTA (1 wt% as crosslinker) and DMPA (1 wt%) were dissolved in methanol to prepare solutions of varying molar ratios of BA and SBMA. The solution was deoxygenated by purging with nitrogen for 30 min before surface grafting to the PDMS-SH. Ultraviolet (UV, 365 nm) irradiation was exposure for 20 min under nitrogen atmosphere to complete the grafting process. Different samples were named as S_xB_y, where the "x" indicates the percentage of SBMA, "y" indicates the percentage of BA (e.g., $S_{50}B_{50}$ refers to a 50 % SBMA and 50 % BA molar ratio). Finally, the samples were washed with methanol to remove any unreacted monomers. The detailed synthesis process is shown in Fig. 1a.

2.3. Characterization

The surface composition of PDMS before and after grafting was characterized using Fourier Transform Infrared Spectroscopy (FTIR, Thermo Fisher Scientific Nicolet iS5, USA) and X-ray photoelectron spectroscopy (XPS, Thermo Scientific K-Alpha, USA). The transmittance of the sample in the visible light wavelength range was measured using UV-Vis (UV-6100, MAPADA, China). The hydrophilicity was evaluated by measuring the water contact angle (WCA, Zhongchen Digital JC 2000 C, China). Surface morphology before and after grafting was examined using scanning electron microscopy (SEM, ZEISS Gemini SEM 300, Germany). Microplate Absorbance Reader (Tecan A-5082 SUNRISE, Austria) was used to assess the MTT results and blood compatibility. Confocal laser scanning microscopy was used to observe cell viability and morphology (CLSM, Leica SP5, Germany).

2.4. Anti-bacterial adhesion assays

The anti-bacterial adhesion assays for different samples were conducted using a previously described method [24]. Briefly, *E. coli* and *S. aureus* were streaked on TSA plates and incubated for 24 h to obtain single colony. The colonies were transferred and cultured in TSB medium on a shaker for 8 h (37 °C, 180 rpm), then centrifuged to remove TSB medium and washed three times with sterile saline to obtain a bacterial suspension. The concentration was adjusted to 10^8 CFUs/mL (Colony Forming Units/mL) for the anti-bacterial adhesion experiment. PDMS with different coatings were immersed in the bacterial suspension and incubated at 37 °C for 24 h. After incubation, the materials were gently rinsed three times with sterile saline to remove non-adherent bacteria. Then the materials were immersed in 1 mL of sterile saline, followed by sonication for 10 min to detach the adherent bacteria. 100 μL solution was spread on TSA plates and incubated for 24 h at 37 °C, after which the bacterial colonies were counted. All materials were sterilized by UV irradiation on both sides for 15 min before use. The anti-adhesion rates were calculate using followed formula.

$$\text{anti} - \text{adhesion rate}(\%) = \frac{A - B}{B} \times 100\% \quad (1)$$

Here, A presents the bacterial CFUs spread on TSA of groups with different coatings, B presents the bacterial CFUs spread on TSA of group PDMS.

2.5. Anti-bacterial biofilm performance assay

To investigate the anti-bacterial biofilm performance of various coatings, biofilms were cultured on the corresponding surfaces. The PDMS with different coatings were placed at the bottom of 48-well plates, with PDMS serving as the control. TSB medium, supplemented with 1 wt% glucose and 5 wt% NaCl, was used to dilute the bacterial suspension to a concentration of 10^6 CFUs/mL. Subsequently, 500 μL of

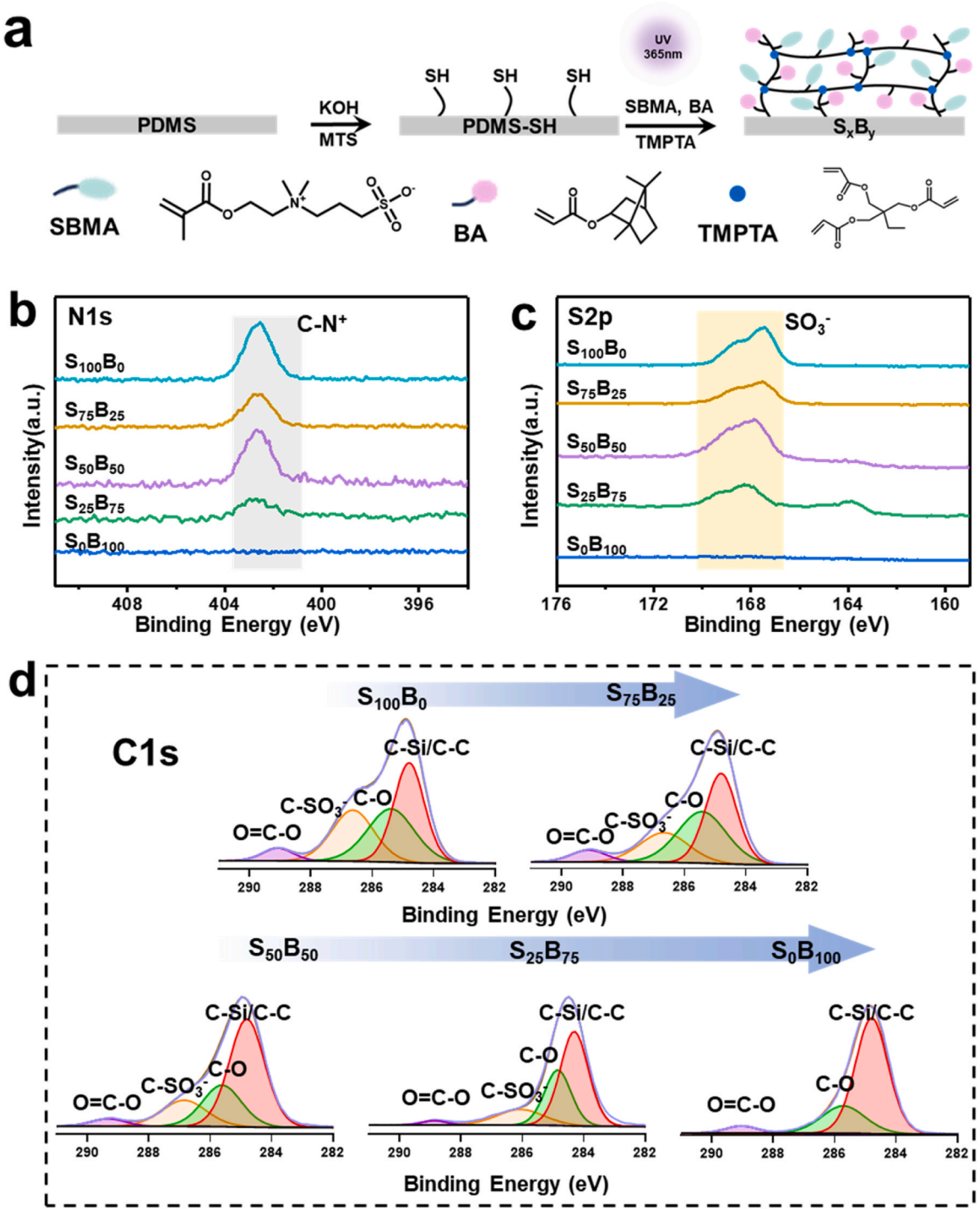

Fig. 1. Synthesis process diagram and XPS spectra of different samples. (a) Synthesis process of S_xB_y. (b) N1s (c) S2p and (d) C1s high-resolution spectrum of S_xB_y.

the bacterial suspension was added to each well, and the volume of the medium was adjusted to 1 mL. The plates were incubated at 37 °C for 24 h in a bacterial incubator. Then, 500 μL of the medium was gently removed to avoid disturbing the biofilm at the bottom, and 500 μL of fresh medium was added. Referring to previously reported culture durations, *S. aureus* was cultured for 24 h and *E. coli* for 48 h to allow the formation of mature biofilms [25–28]. After incubation, the medium was removed and replaced with sterile saline solution, which was used to gently rinse and remove any free bacteria, thus obtaining biofilm-contaminated material surfaces.

The biofilm was then performed to a staining procedure utilizing a crystal violet solution (1 mg/mL in deionized water). 500 μL of the crystal violet solution was added to each biofilm-contaminated well and incubated in the bacterial incubator for 30 min. Subsequently, the solution was then removed, and the wells were gently rinsed three times with saline to remove excess stain, leaving stained biofilms behind. Finally, 30 % acetic acid in anhydrous ethanol (v/v) was added to each well and shaken at 90 rpm for 15 – 20 min to dissolve the crystal violet. After diluting the solution, the absorbance was measured at optical density (OD) 595 nm using a microplate reader. The bacterial biofilm biomass was calculated using the following formula:

$$\text{Biofilm biomass}(\%) = \frac{A}{B} \times 100\% \quad (2)$$

Here, A presents the absorbance at 595 nm (OD 595) of groups with different coatings, B presents the OD 595 of group PDMS.

2.6. Anti-mold adhesion properties

The anti-mold adhesion properties were evaluated using a "landing model" [29]. Briefly, the sterilized materials were placed on the surface of malt agar plates, with sterile filter paper placed about 2 cm away. Then, 7 μL of an *A. niger* spore suspension in saline ($1 - 5 \times 10^8$ spores/mL) was added to the filter paper. The plates were incubated in a mold growth chamber for 7 d (30 °C, relative humidity of 85 % ± 5 %), after which mold contamination on the material surface was monitored and photographed. ImageJ software was used for quantitative analysis of the contaminated area on the material surface.

2.7. Anti-mold biofilm performance assay

The experimental method for anti-mold biofilm assessment was adapted and improved from previously reported [30]. Briefly, PDMS substrates with different coatings were placed at the bottom of a 24-well plate. Each well was then filled with 2 mL of RPMI 1640 medium containing 10^5 spores mL^{-1} and supplemented with 2 wt% glucose, with uncoated PDMS serving as the control group. Referring to previously reported culture durations, the plates were incubated in a mold incubator at 30 °C for 48 h to obtain mature mold biofilms [31,32]. After incubation, the culture medium was gently removed, and the substrates were rinsed carefully with sterile physiological saline to obtain materials contaminated with mold biofilms. Subsequently, 1 mL of 0.1 wt% crystal violet solution was added to each well and incubated at 37 °C for 1 h for staining. The substrates were then rinsed gently three times with sterile physiological saline to yield crystal violet-stained biofilms. Finally, the biofilms were washed with 30 % (v/v) acetic acid in ethanol under gentle agitation at 90 rpm for 1 h. The absorbance of the washing solution was measured at OD 595 nm. The mold biofilm biomass was calculated using the following formula:

$$\text{Biofilm biomass}\ (\%) = \frac{A}{B} \times 100\% \quad (3)$$

Here, A presents the absorbance at 595 nm (OD 595) of groups with different coatings, B presents the OD 595 of group PDMS.

2.8. Antimicrobial mechanism evaluation

For mold, a previously reported "contact killing" experiment was conducted [33]. In brief, 20 μL spore suspension of *A. niger* (10^8 CFUs/mL) was dropped between sterilized samples to form a sandwich model. The model was then placed in a blank petri dish, with deionized water added around the edges to prevent spore desiccation. The setup was sealed and incubated in a fungal incubator for 24 h to complete the co-cultivation process. Finally, the side in contact with *A. niger* was placed in the center of a malt extract agar plate (marked as "×"), and photographs were taken to monitor the growth condition of *A. niger*.

For bacteria, The anti-bacterial inhibition zone (ZOI) test was performed as previously described [34]. Before the experiment, the materials were sterilized by UV irradiation (15 min on each side). 100 μL bacterial suspension (10^7 CFU/mL) was spread onto the surface of TSA agar. The coating side of the material was placed face-down onto the agar, and the plates were incubated in a bacterial incubator for 24 h. After incubation, photographs were taken to observe any zones of inhibition.

2.9. In vitro biocompatibility evaluation

The biocompatibility of different materials was evaluated using the MTT assay [35]. Sterilized materials were immersed in 1 mL of RPMI 1640 medium (10 % FBS, 100 μg mL^{-1} penicillin, and 100 μg mL^{-1} streptomycin) and incubated at 37 °C in a cell incubator (95 % air, 5 % CO_2) for 24 h to obtain the material extracts (the leachable fraction that is released into the extraction medium during the incubation process). Mouse L929 fibroblast cells were used for the biocompatibility evaluation. The cells were cultured to the logarithmic growth phase and then resuspended in fresh RPMI 1640 medium. Cells were seeded into 96-well plates at a density of 8000 cells per well in 100 μL of medium and incubated for 24 h. Next, 100 μL of the material extracts replaced the 1640 medium, and incubation continued for another 24 h. Each well was then treated with 10 μL of MTT solution (5 mg mL^{-1} in PBS) and incubated for an additional 4 h. The assay was terminated by adding 100 μL of 10 % SDS to dissolve the formazan crystals overnight at room temperature. Absorbance was measured at 570 nm using a microplate reader. Cell viability was calculated using the following formula:

$$\text{Cell viability}\ (\%) = \frac{Abs_{sample} - Abs_{control}}{Abs_{cell} - Abs_{control}} \times 100\% \quad (4)$$

Abs_{sample} represents the absorbance of cells cultured with the material extracts. $Abs_{control}$ refers to the absorbance of blank RPMI 1640 medium, and Abs_{cell} represents the absorbance of cells cultured in RPMI 1640 medium under the same conditions.

2.10. Blood compatibility evaluation

Blood compatibility was assessed using a previously reported method [36]. 1 mL of anticoagulated whole blood was added to 2 mL of phosphate-buffered saline (PBS, pH 7.4) and centrifuged at 500 G for 10 min to remove the supernatant. Then the PBS was added back to a final volume of 3 mL, and the mixture was centrifuged again. This washing process was repeated five times. After the final centrifugation, the supernatant was discarded, the remaining solution was diluted to 10 mL with PBS to obtain a red blood cell suspension (RBCs). Next, 0.2 mL of RBCs was transferred into 1.5 mL centrifuge tubes, and the volume was adjusted to 1 mL with PBS. Different materials were then placed into different centrifuge tubes, with no treatment as the blank group, PBS group as the negative control, and triton solution group as the positive control. The samples were incubated at 37 °C on a shaker for 3 h. After incubation, the samples were removed, centrifuged at 10, 000 G for 5 min, and 100 μL of the supernatant was collected. The OD was measured at 540 nm. The hemolysis ratio was calculated using the following formula:

$$\text{Hemolysis ratio}\ (\%) = \frac{A_{sample} - A_{negative}}{A_{positive} - A_{negative}} \times 100\% \quad (5)$$

A_{sample} is the absorbance of the RBCs supernatant after incubation with different samples, $A_{negative}$ is the absorbance of the PBS treated RBCs supernatant, and $A_{positive}$ is the absorbance of the triton solution treated RBCs supernatant.

2.11. In vivo biocompatibility evaluation

The *in vivo* biocompatibility assessment was performed using a subcutaneous implantation model in mice. Materials were sterilized by UV 15 min for each side of materials. Before implantation, hair removal cream was applied to the mice to remove fur. After implantation, the incision was sutured. On day 5, the mice were euthanized by cervical dislocation, and the subcutaneous tissue was collected for histological analysis using hematoxylin and eosin (H&E) staining to examine the surrounding tissue.

Animal handling and care followed the guidelines outlined in the National Research Council's Guide for the Care and Use of Laboratory

Animals and were supervised by the SPF Animal Department of the Clinical Institute at the China-Japan Friendship Hospital (Approval No. Zryhyy 12–20–08–3).

2.12. Significance testing

Data are presented as mean ± SD. Statistical significance was evaluated using *t*-test. ns, $p > 0.05$, $^{*}p < 0.05$, $^{**}p < 0.01$, $^{***}p < 0.001$, $^{****}p < 0.0001$.

3. Result and discussion

3.1. Chemical structure characterization

Thiol-modified PDMS serves as the substrate, using thiol-ene click chemistry under 365 nm UV light to form polymer coatings with varying SBMA/BA ratios. To ensure the stability of the coating, TMPTA was selected as the cross-linking agent to form a cross-linked network. Owing to its trifunctional acrylate groups, TMPTA can form a more stable three-dimensional network compared to difunctional acrylate-based cross-linkers (such as polyethylene glycol diacrylate), while also exhibiting good biocompatibility [37,38]. Fig. 1a illustrates PDMS-SH and S_xB_y synthesis process. FTIR was used to investigate the chemical structure of different coatings (Fig. S1). Since both monomers belong to acrylate, they have a characteristic C═C bond. The absorption peak of the C═C double bond at 1637 cm^{-1}, which corresponds to the characteristic absorption peaks of the two unreacted monomers, was not observed in all experimental groups. This proved that the monomers reacted sufficient and did not remain on the surface of the material. Compared with the PDMS group, the absorption peak at 1735 cm^{-1} is significantly enhanced, which corresponds to the vibration of the C═O ester bond in the acrylate structure [39]. This observation provides preliminary evidence of the two monomers' successful polymerization at the surface of the substrate. The symmetric and asymmetric vibrations of SO_3^- in sulfobetaine are represented by 1033 cm^{-1} and 1167 cm^{-1}. The quaternary ammonium structure absorption peaks of sulfobetaine are represented by 1480 cm^{-1}. The corresponding absorption peaks can be observed in the groups with the addition of SBMA [40]. The C–H vibration can be observed at 2960 cm^{-1} [22], corresponding to the methyl groups in both borneol and sulfobetaine.

XPS was used to further investigate the composition of different coatings. Under alkaline conditions, MTS was hydrolyzed and covalently bonded to the surface of PDMS to form PDMS-SH. Compared with the PDMS group, a thiol characteristic peak can be observed at 163.9 eV in the S2p element high-resolution spectrum (Fig. S2a), and enhanced C–S and C–O bond characteristic peaks can be seen at 285.7 eV (Fig. S2b), proving the successful synthesis of the first step PDMS-SH [41,42]. Subsequently, under 365 nm UV light exposure, the surface grafting of the two monomers (SBMA and BA) was achieved through thiol-ene click chemistry. Fig. 1b presents the high-resolution N1s spectra of different samples. Characteristic peaks indicative of nitrogen-related chemical bonds was not detected in the S_0B_{100} group, indicating the absence of such bonds. However, in the $S_{25}B_{75}$, $S_{50}B_{50}$, $S_{75}B_{25}$, and $S_{100}B_0$ groups, an characteristic peak around 402.5 eV corresponding to $C–N^+$ was observed [43]. Similar results were found in the high-resolution at S2p spectra, where the S_0B_{100} group showed no distinct characteristic peaks, while the $S_{25}B_{75}$, $S_{50}B_{50}$, $S_{75}B_{25}$, and $S_{100}B_0$ groups displayed an characteristic peak at approximately 167.7 eV, associated with the SO_3^- structure (Fig. 1c) [44]. The presence of $C–N^+$ and SO_3^- structures, which are characteristic of SBMA, provides further evidence confirming the successful synthesis of the coating. The detailed analysis of carbon-related chemical bonds through the C1s spectra (Fig. 1d) reveals significant results. Compared with the control group, all coatings have showed a characteristic peak around 288.8 eV, corresponding to O═C–O bonds, and another peak at 285.5 eV were observed, related to C–O bonds. These structures are characteristic of ester bonds found in the two acrylate monomers. The distinct $C–SO_3^-$ at 286.3 eV structure specific to SBMA was identified in the $S_{100}B_0$, $S_{75}B_{25}$, $S_{50}B_{50}$, $S_{25}B_{75}$ groups [45]. As the proportion of SBMA decreased, this characteristic peak showed a gradual decline trend. In the S_0B_{100} group, the characteristic peak for $C–SO_3^-$ disappeared, whereas ester bond peaks derived from the BA monomer grafted onto the PDMS surface remained.

The combined FTIR and XPS results confirm the successful grafting of SBMA and BA monomers onto the PDMS substrate through thiol-ene click chemistry. The presence of characteristic chemical bonds associated with SBMA and BA, and their proportional changes, further validate the synthesis of coatings with varying SBMA/BA ratios.

3.2. Surface morphology and hydrophilicity

Surface properties are crucial parameters for evaluating coatings. The surface morphology and hydrophilic properties of the different samples are shown in Fig. 2. Fig. 2a illustrates the macroscopic images of the various samples. The untreated PDMS exhibits high transparency, whereas the PDMS-SH and grafted coating samples display reduced transparency. The coatings containing SBMA surfaces appear relatively smooth, while the S_0B_{100} sample exhibits a rough surface, likely due to the rigidity of the poly(borneol acrylate) and its incompatibility with the elastic PDMS substrate. The transmittance of different samples in the visible light range was further tested (Fig. S3). Similar results can be obtained. The PDMS exhibits the highest transparency, reaching 90 % in the visible light range. In contrast, the PDMS-SH demonstrates the lowest transparency, with a value of approximately 10 %. The S_0B_{100} coating exhibits a slightly enhanced transparency, reaching approximately 40 %. The coatings containing SBMA demonstrated enhanced visible light transmittance, with transmittance exceeding 60 %. This finding demonstrates that zwitterionic units are critical in enhancing the optical transparency of the coating [46,47]. Fig. 2b shows the contact angle results of different samples. PDMS showed hydrophobic properties with a contact angle of 106°, which decreases to 81° after thiol modification, likely due to the presence of –SH groups on the surface. The contact angles of the $S_{100}B_0$, $S_{75}B_{25}$, $S_{50}B_{50}$, $S_{25}B_{75}$, S_0B_{100} samples are 27°, 72°, 78°, 84°, and 105°, respectively. S_0B_{100} exhibited hydrophobic characteristics, while $S_{100}B_0$ was hydrophilic. As the BA content increased and the SBMA content decreased (from $S_{100}B_0$ to S_0B_{100}), the material demonstrated a trend of progressively enhanced hydrophobicity. This trend is attributed to dipole interactions between ionic groups in SBMA and polar water molecules, which enhance the coating's hydrophilicity. As BA content increases, more hydrophobic carbon cage structures are introduced, leading to a gradual increase in WCA.

SEM was used to further examine the surface morphology (Fig. 2c). The PDMS displayed a smooth surface, while the surface of the PDMS-SH exhibited small amount particulate structures, likely resulting from the hydrolytic reacted behaviors of MTS intermolecular [48]. All samples exhibited a relatively smooth structure, confirming the stable presence of the crosslinked coating on the PDMS surface. Notably, compared to the coatings containing zwitterionic, The S_0B_{100} surface displayed slightly protrusions in its surface morphology, consistent with macroscopic observations. This indicates that the introduction of zwitterionic hydrophilic units contributes to enhancing the smoothness of the coating surface [49]. Further SEM observations of the samples cross-sections were conducted (Fig 2d). It was found that PDMS and PDMS-SH showed no obvious coating structure. In contrast, S_xB_y exhibited a distinct coating structure with a thickness of approximately 2 μm. Moreover, no apparent gaps were observed between the coating and the substrate, indicating that the coating was stably grafted onto the PDMS surface. These SEM results provide direct evidence of the successful synthesis of the coating.

3.3. Anti-mold adhesion properties

The anti-mold evaluation of different materials was performed using

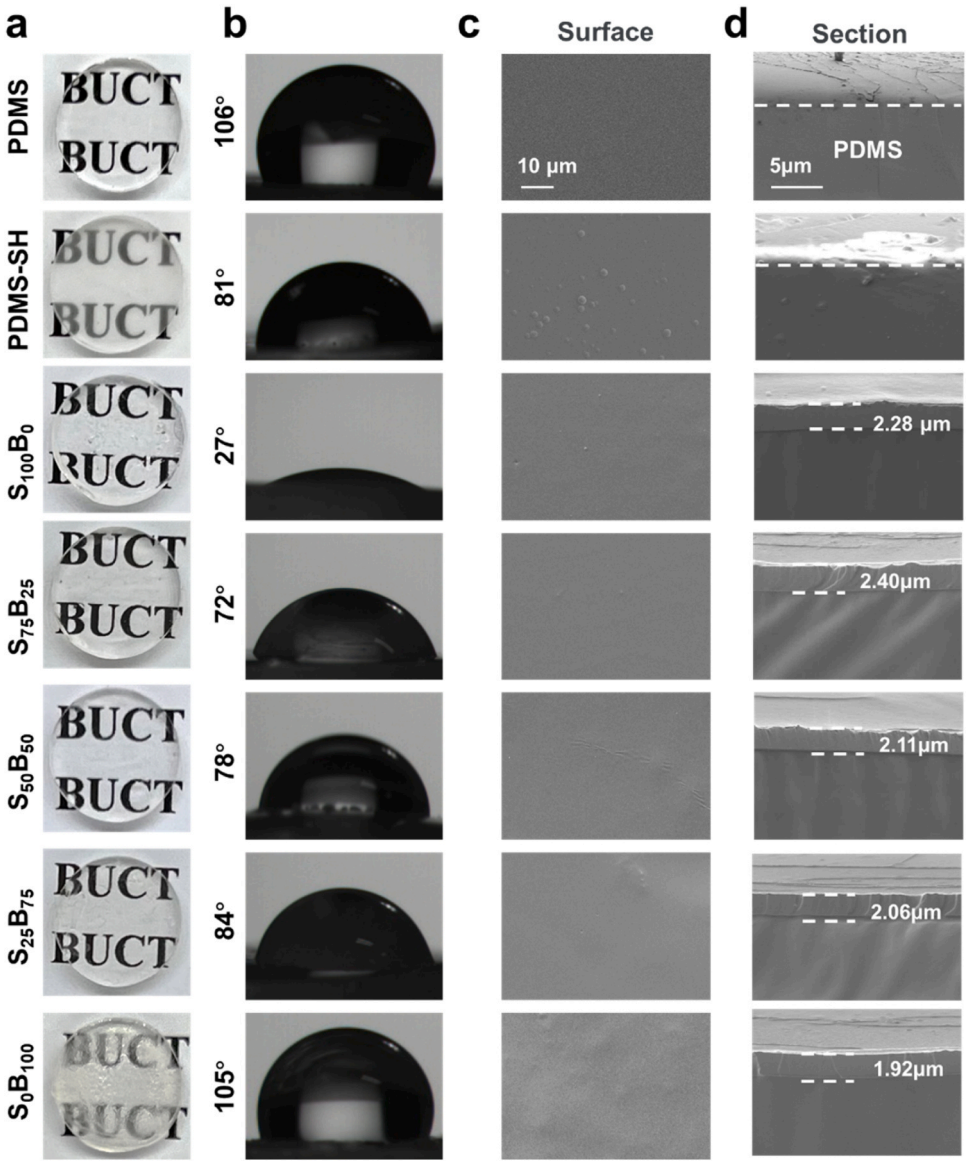

Fig. 2. Surface morphology and hydrophilicity characterization of different samples. (a) photograph of different samples. (b) The water contact angle image of different samples. (c) The SEM (c) surface and (d) section images of different samples.

"landing model". Fig. 3a shows a schematic diagram of the "landing model". A sterile filter paper sheet was attached to the middle of the culture medium and a spore solution was dripped on its surface. Then the material was attached to a position about 2 cm from the center. Fig. 3b shows the growth process of *A. niger* and surface contamination condition magnified images. After 7 days, the magnified view was used to observe *A. niger* contamination on the material surface. When *A. niger* grows to the material surface, an anti-adhesive surface can inhibit its further colonization and growth. In contrast, the surface without resistance to *A. niger* adhesion will be contaminated by climbing to the material surface. After 7 days, the surfaces of the PDMS and the $S_{100}B_0$ group were contaminated by *A. niger* and invaded the center of the material, indicating that the PDMS and zwitterionic SBMA coatings have no obvious anti-mold ability. As the amount of borneol units increased, the *A. niger* contaminated area gradually decreased, for $S_{75}B_{25}$ coating, only the edge was contaminated, while the middle was not contaminated (inside the yellow circle). The surfaces of $S_{50}B_{50}$, $S_{25}B_{75}$ and S_0B_{100} coatings were not obvious contaminated by *A. niger*. Fig. 3c presents the statistical data on *A. niger* contamination on different material surfaces. The PDMS surface exhibited the highest contamination area at 13.25 %. The $S_{100}B_0$ and $S_{75}B_{25}$ groups showed varying degrees of contamination at 4.80 % and 0.53 %, respectively. In contrast, the $S_{50}B_{50}$, $S_{25}B_{75}$, and S_0B_{100} groups showed no obvious contamination by *A. niger*, and there were no significant differences among these three groups. Therefore, it is proved that with the increase of the addition amount of BA, the anti-mold adhesion performance of the coating gradually increased. When the addition amount of BA is greater than 50 %, the coating surface is not contaminated by *A. niger* and has great anti-mold performance.

Crystal violet staining method was designed to further evaluate the anti-mold performance (Fig 4a). For the PDMS group, pronounced biofilm biomass was observed on the surface, indicating its inability to prevent mold biofilm formation. In contrast, all S_xB_y groups exhibited a reduction in biofilm biomass (Fig 4b). Further statistical analysis revealed that the biofilm biomass for $S_{100}B_0$, $S_{75}B_{25}$, $S_{50}B_{50}$, $S_{25}B_{75}$, and S_0B_{100} were 41.6 %, 18.7 %, 19.6 %, 26.4 %, and 23.0 %, respectively (Fig. 4c). While $S_{100}B_0$ demonstrated mold biofilm inhibition, its effect was the weakest compared to coatings containing borneol groups. Thus, the addition of BA effectively suppresses mold biofilm formation. This result further confirms the critical role of the borneol structure in mold

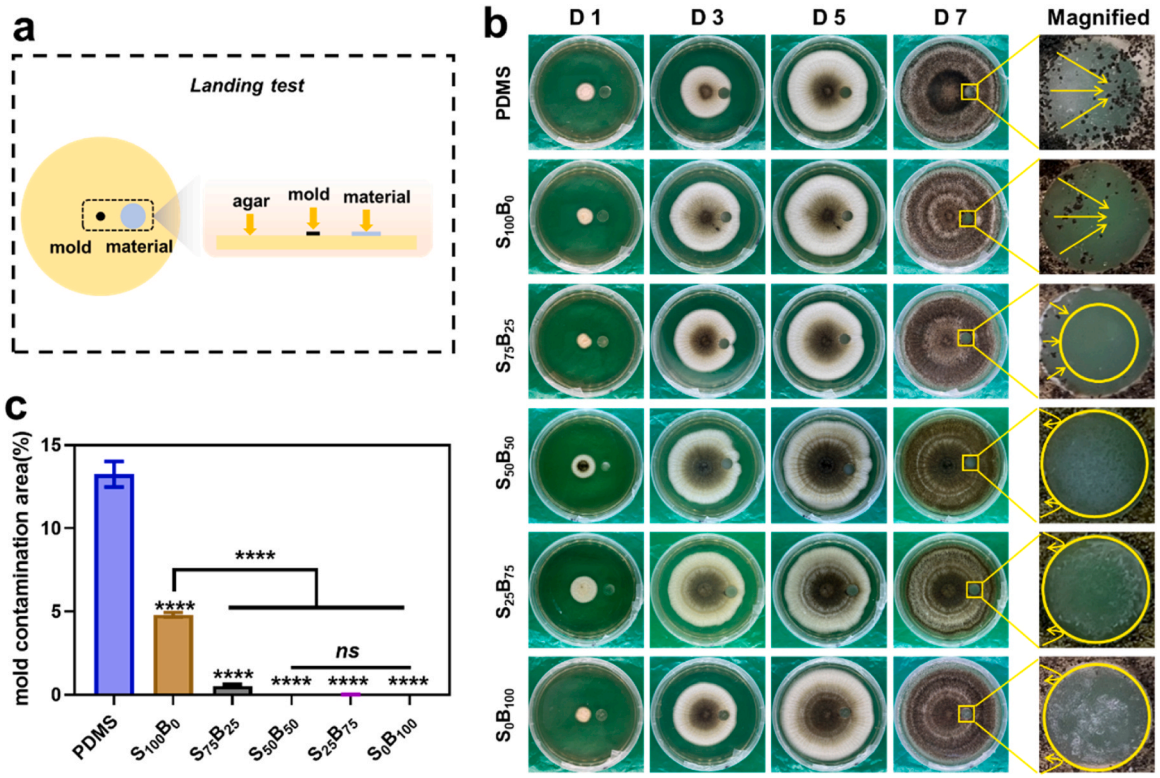

Fig. 3. The results of anti-mold adhesion properties. (a) Schematic diagram of the "landing test". (b) Images of mold growth and contamination on sample surfaces. (c) Mold contamination area statistics. ****$p < 0.0001$.

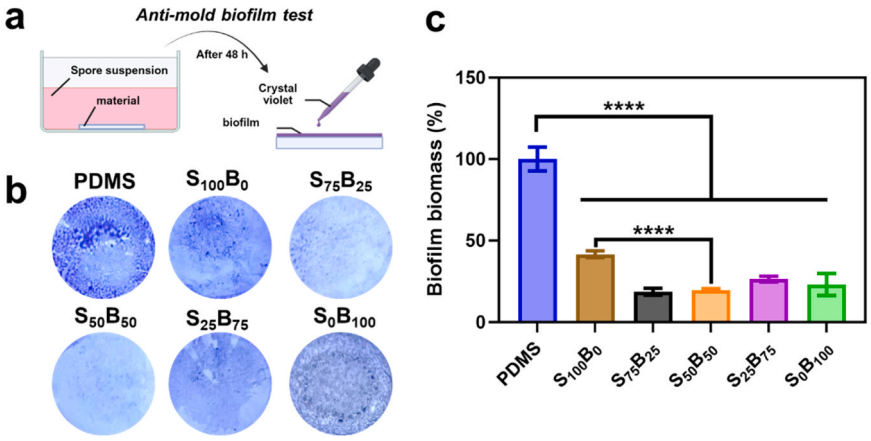

Fig. 4. The results of anti-mold biofilm properties. (a) Schematic diagram of "anti-mold biofilm test". (b) Images of mold biofilm biomass results. (c) Mold biofilm biomass statistics. ****$p < 0.0001$, ns, $p > 0.05$.

biofilm formation.

3.4. Anti-bacterial adhesion properties

The anti-bacterial properties of S_xB_y were evaluated. Fig. 5a shows the images of bacterial colony count on the surfaces of different coatings after co-culture with bacterial suspensions spread on the TSA plates. Fig. 5b and Fig. 5c present statistical analyses of *E. coli* and *S. aureus* adhesion on the different material surfaces. All coatings display effective anti-bacterial adhesion properties. For *E. coli*, the anti-adhesion rates for $S_{100}B_0$, $S_{75}B_{25}$, $S_{50}B_{50}$, $S_{25}B_{75}$, and S_0B_{100} were 92.9 %, 98.7 %, 97.5 %, 95.5 %, and 90.9 %, respectively. For *S. aureus*, the anti-adhesion rates were 94.3 %, 92.5 %, 96.8 %, 95.4 %, and 91.8 %, respectively. It is noteworthy that different ratios of SBMA/BA additions appeared to exhibit synergistic anti-bacterial adhesion trends. This may be attributed to the formation of a hydration layer by hydrophilic zwitterions in aqueous environments, which inhibits initial bacterial adhesion. However, bacteria that overcome this barrier may recognize the distinctive stereochemistry of borneol, thereby deterring further adhesion. Therefore, the combination of zwitterions and borneol represents a potential strategy for achieving anti-bacteria adhesion synergistic effects.

The formation of biofilms on material surfaces, which are challenging to remove, is a major and persistent cause of infection. To further investigate the anti-biofilm performance of S_xB_y under complete medium conditions, an anti-bacterial biofilm formation assay was conducted. Fig. 6a presents the images of *E. coli* and *S. aureus* biofilm biomass on different groups after incubation. Fig. 6b and Fig. 6c show the statistical analysis of *E. coli* and *S. aureus*, respectively. It can be

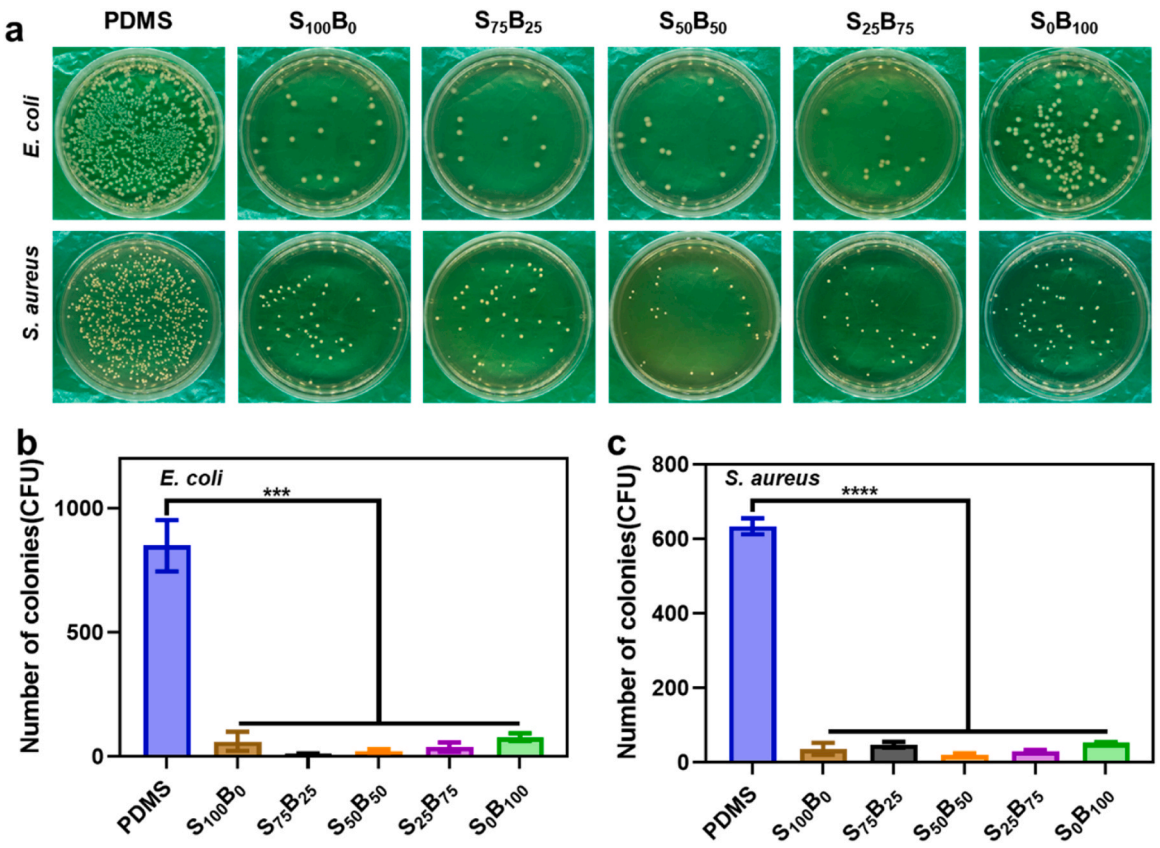

Fig. 5. The results of anti-bacterial adhesion assay. (a) Plates photographs after bacterial co-culture. The CFUs number statistics of (b) *E. coli* and (c) *S. aureus*. ***$p < 0.001$, ****$p < 0.0001$.

observed that the PDMS group exhibits a notable degree of biofilm coverage and does not display resistance to biofilm adhesion. For *E. coli*, the biofilm biomass on $S_{100}B_0$, $S_{75}B_{25}$, $S_{50}B_{50}$, $S_{25}B_{75}$, and S_0B_{100} coatings was 25.9 %, 15.1 %, 10.7 %, 16.3 % and 37.4 %, respectively. Similarly, for *S. aureus*, the corresponding values were 42.7 %, 31.8 %, 20.4 %, 61.9 % and 77.1 %. Although all coatings exhibited excellent anti-bacterial adhesion properties, there were notable differences in their ability to inhibit biofilm formation. It is noteworthy that, The S_0B_{100} coating does not exhibit ideal performance in anti-biofilm formation. Nonetheless, the anti-bacterial biofilm effect was gradually enhanced with the increase of SBMA addition and even demonstrated synergistic anti-biofilm effect, both against *E. coli* and *S. aureus*. This finding was a surprise to us. It is likely due to the borneol large hydrophobic cyclic carbon cage structure that renders the surface hydrophobic, shows the ineffective at preventing protein adhesion. The addition of SBMA addresses this limitation. The SBMA/BA ratio of 1:1 exhibits the highest anti-biofilm efficacy among all groups. This enhanced effect is attributed to sulfobetaine strong hydrophilicity, which inhibits protein adhesion and reduces bacterial proliferation on the surface. Furthermore, borneol's distinctive stereochemical structure interferes with bacterial recognition, and together with SBMA, forms a unique bimolecular coating that exhibits optimal anti-biofilm efficacy.

In summary, based on the results of anti-bacterial adhesion, anti-mold and anti-biofilm, we selected the optimal $S_{50}B_{50}$ coating for subsequent experiments. To further explored the antimicrobial mechanism of the coating, "contact killing" and ZOI experiment was designed. Fig. S4a shows the contact killing process diagram. If the material surface lacks killing mold activity, mold spores can germinate and grow. Fig. S4b illustrates the growth states of *A. niger* at different time points, demonstrating its ability to grow normally. For bacteria, both *S. aureus* and *E. coli*, no obvious inhibition area was observed (Fig. S5). These results further proved that the $S_{50}B_{50}$ coating is not through releasing small molecules, but by "anti-adhesion" mechanism to achieved its antimicrobial effect.

3.5. Antimicrobial mechanism

The antimicrobial mechanism of the S_xB_y coatings is systematically analyzed to enhance understanding of this work (Fig. 7). A cooperative effect between hydrophilic zwitterionic sulfobetaine and hydrophobic stereochemically borneol functional groups, accounts for the antimicrobial properties of the S_xB_y coatings. Sulfobetaine groups form a surface hydration layer that effectively resists initial bacterial adhesion and protein adsorption, thereby inhibiting biofilm formation. However, their anti-mold adhesion effect is relatively limited due to the hydrophilic surface. Borneol groups has bulky cyclic structure, disrupts microbial recognition and impedes mold adhesion. Although borneol groups enhance anti-adhesion properities, hydrophobicity surface may cause protein adhesion, which subsequently leads to bacterial biofilm formation. The introduction of sulfobetaine groups imparts hydrophilic characteristics to the coatings, as evidenced by WCAs below 90°. Optimal antimicrobial performance at a 1:1 SBMA/BA ratio suggests that a balanced combination of surface hydration and stereochemical interference maximizes both antibacterial and anti-mold efficacy. This continuous dual-functional coating strategy offers a promising approach for long-term biofouling resistance.

3.6. Biocompatibility

Biocompatibility is a crucial evaluation criterion for materials used in the medical field. The samples were evaluated by *in vitro* cytocompatibility and hemocompatibility (Fig. 8). Fig. 8a shows the fluorescence images of different samples after co-culture with cells for 24 h. Cells treated with culture medium were used as the control group. All

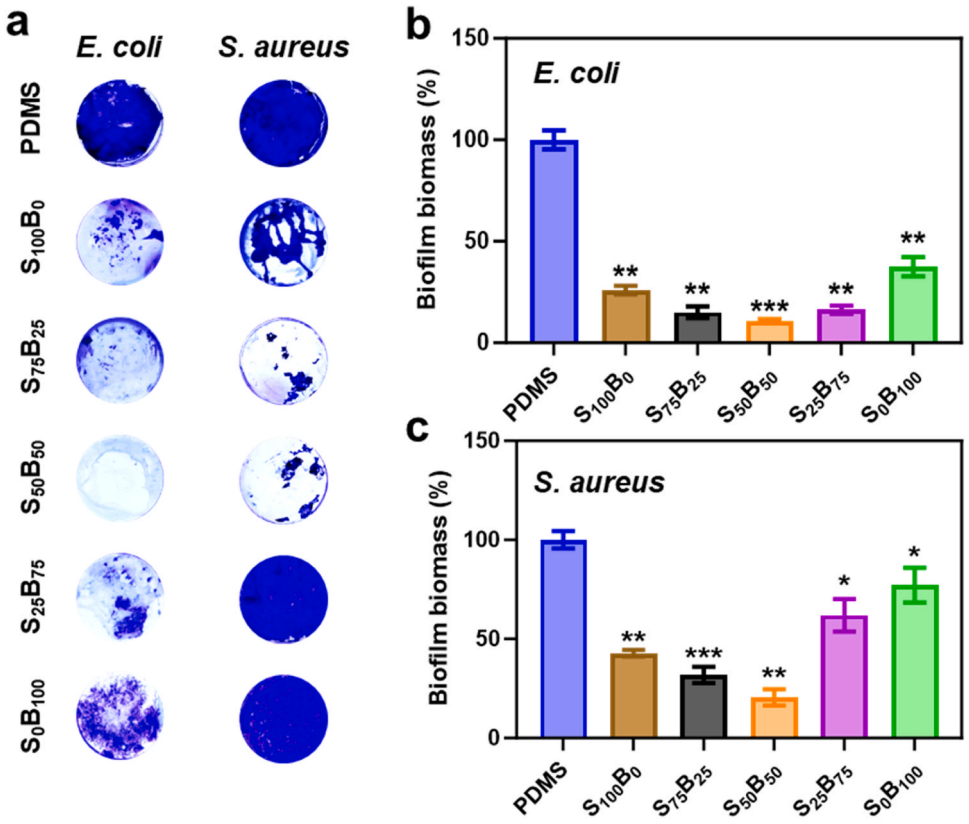

Fig. 6. The anti-biofilm results. (a) The biofilm biomass images of different samples for *E. coli* and *S. aureus*. The statistical analyses of biofilm biomass for (b) *E. coli* and (c) *S. aureus*. *$p < 0.05$, **$p < 0.01$, ***$p < 0.001$.

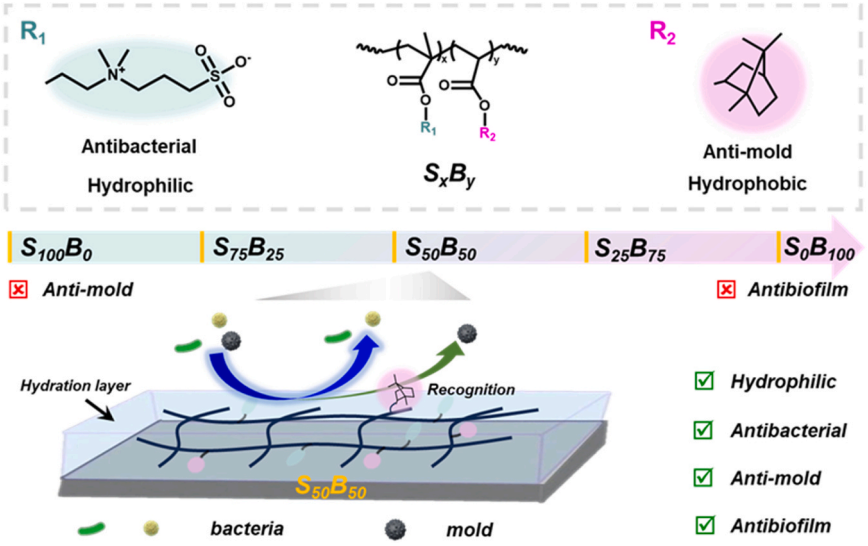

Fig. 7. Schematic diagram of antimicrobial mechanism.

L929 cells showed clear outline and appeared spindle-shaped. The cytocompatibility of the samples was further evaluated using the MTT method (Fig. 8b), all cells cultured with the sample extracts showed good cell viability (>95 %), and there was no significant difference compared with the control group. Fig. 8c shows the hemolysis rate results. PBS and triton were selected as the negative control group and the positive control group, the hemolysis rate of the $S_{50}B_{50}$ sample was less than 5 %, demonstrating that the sample had good blood compatibility. Additionally, a mice subcutaneous implantation model was further utilized to verify the *in vivo* safety of the samples. Fig. 8d presents the results of H&E staining of the surrounding tissue after 5 days implantation. Compared with the control group, the $S_{50}B_{50}$ group also showed no significant inflammatory cells in the surrounding tissue, indicating that the material did not cause *in vivo* dormant bacterial aggregation or subsequent infection, confirming its good *in vivo* histocompatibility. Therefore, the results of both *in vitro* and *in vivo* biocompatibility evaluations demonstrate that the $S_{50}B_{50}$ coating possesses excellent safety, indicating its potential for application in medical implants.

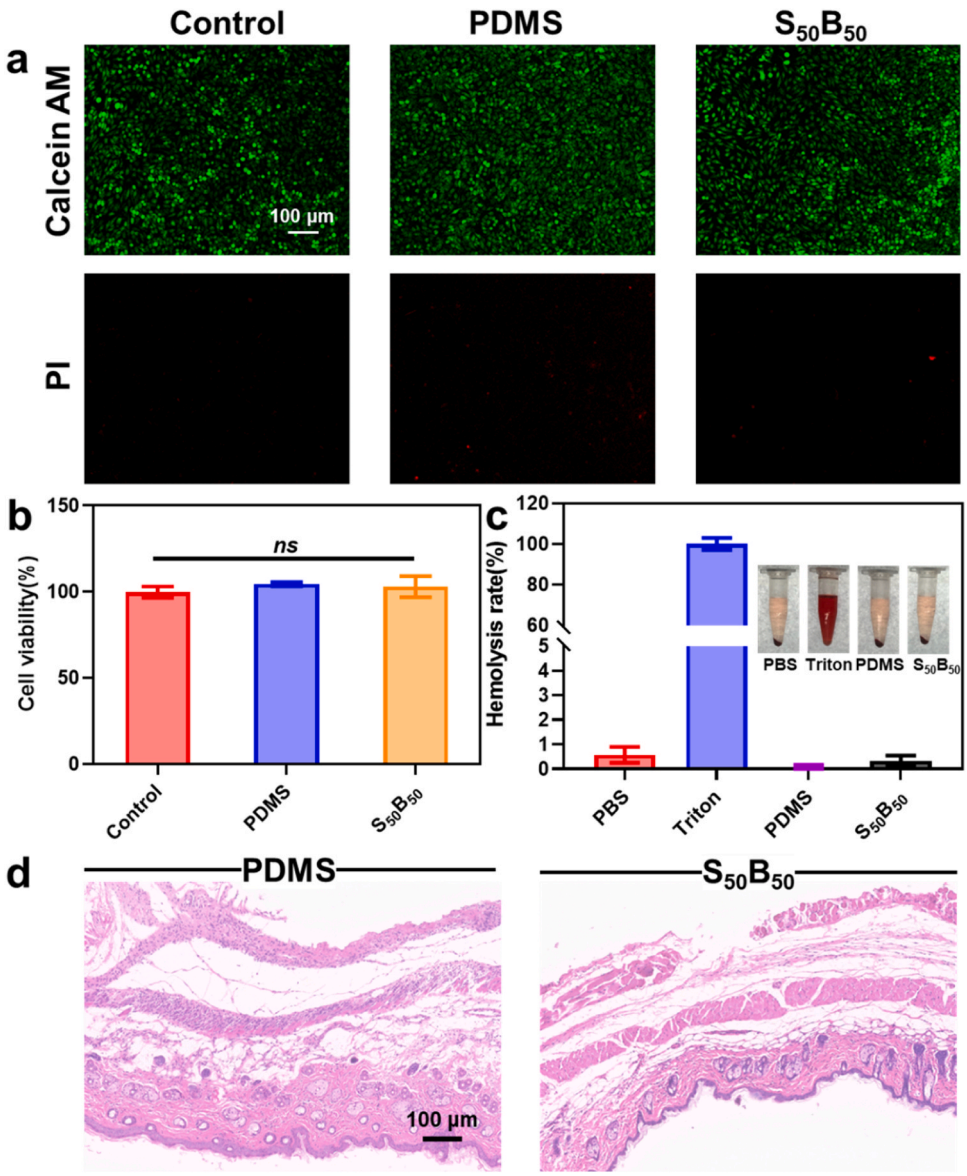

Fig. 8. Biocompatibility evaluation. (a) Calcein AM/PI staining images of L929 cells after 24 h incubation with different samples. (b) Cell viability assay by MTT method. (c) Hemolysis rates of different samples and their hemolysis results (inside graph). (d) H&E staining results of surrounding tissues. ns, $p > 0.05$.

4. Conclusion

In conclusion, we employed a thiol-ene click chemistry approach to modify the surface of the PDMS with a zwitterionic/borneol bimolecular coating. The results showed that the addition ratio of SBMA/BA played a vital role in regulating the resistance to microbial contamination. By adjusting the ratio of SBMA to BA to 1:1, we achieved excellent anti-bacterial adhesion, anti-mold adhesion and anti-biofilm formation properties. *In vitro* cytotoxicity and hemolysis assays demonstrated good cytocompatibility and blood compatibility, while further *in vivo* subcutaneous implantation in mice confirmed its superior histocompatibility. Compared with conventional biocidal coatings (e.g., silver ions, antibiotics, quaternary ammonium compounds), which may raise concerns about cytotoxicity and resistance, and anti-adhesion polyethylene glycol/zwitterionic coatings with limited anti-mold activity, the $S_{50}B_{50}$ coating integrates hydrophilic sulfobetaine and hydrophobic borneol into a continuous, non-releasing network that provides broad-spectrum resistance to both bacterial and mold adhesion. However, microorganisms passively adhering to the surface remain difficult to eliminate, indicating that incorporating non-releasing bactericidal functional groups based on this study could represent a potential direction for future research. Overall, the zwitterionic/borneol coating modification strategy provides new insights into the development of antimicrobial strategies for medical devices and implanted materials, particularly in preventing surface biofilm formation.

CRediT authorship contribution statement

Chen Chen: Writing – original draft, Validation, Investigation, Formal analysis, Data curation. **Songtao Wang:** Software, Methodology. **Wenjing Niu:** Validation. **Fang Liu:** Resources. **Wensheng Xie:** Methodology. **Guofeng Li:** Writing – review & editing, Supervision, Funding acquisition. **Dongsheng Kong:** Writing – review & editing, Software, Mehtodology. **Xing Wang:** Writing – review & editing, Supervision, Funding acquisition, Conceptualization.

Supporting information

The FTIR spectrum, transmittance in the visible light range, antimicrobial mechanism results, and high-resolution S2p and C1s spectra of

PDMS and PDMS-SH can be found in the supplementary data.

Declaration of Competing Interest

The authors declare that they have no known financial or personal conflicts of interest that could have appeared to influence the work reported in this paper.

Acknowledgments

This work was supported by the National Natural Science Foundation of China (52273118, 22275013), the Fundamental Research Funds for the Central Universities (QNTD2023–01).

Appendix A. Supporting information

Supplementary data associated with this article can be found in the online version at doi:10.1016/j.colsurfb.2025.114929.

Data availability

Data will be made available on request.

References

[1] S. Edwardson, C. Cairns, Nosocomial infections in the ICU, Anaesth. Intensive Care Med. 20 (2019) 14–18, https://doi.org/10.1016/j.mpaic.2018.11.004.
[2] O. Ciofu, C. Moser, P.Ø. Jensen, N. Høiby, Tolerance and resistance of microbial biofilms, Nat. Rev. Microbiol 20 (2022) 621–635, https://doi.org/10.1038/s41579-022-00682-4.
[3] M.A. Rather, K. Gupta, P. Bardhan, M. Borah, A. Sarkar, K.S.H. Eldiehy, S. Bhuyan, M. Mandal, Microbial biofilm: a matter of grave concern for human health and food industry, J. Basic Microbiol. 61 (2021) 380–395, https://doi.org/10.1002/jobm.202000678.
[4] The Lancet, Antimicrobial resistance: an agenda for all, The Lancet 403 (2024) 2349. https://doi.org/10.1016/S0140-6736(24)01076-6.
[5] Z. Li, X. Yang, H. Liu, X. Yang, Y. Shan, X. Xu, S. Shang, Z. Song, Dual-functional antimicrobial coating based on a quaternary ammonium salt from rosin acid with *in vitro* and *in vivo* antimicrobial and antifouling properties, Chem. Eng. J. 374 (2019) 564–575, https://doi.org/10.1016/j.cej.2019.05.208.
[6] Y. Zhao, L. Shi, X. Ji, J. Li, Z. Han, S. Li, R. Zeng, F. Zhang, Z. Wang, Corrosion resistance and antibacterial properties of polysiloxane modified layer-by-layer assembled self-healing coating on magnesium alloy, J. Colloid Interface Sci. 526 (2018) 43–50, https://doi.org/10.1016/j.jcis.2018.04.071.
[7] J. He, J. Chen, G. Hu, L. Wang, J. Zheng, J. Zhan, Y. Zhu, C. Zhong, X. Shi, S. Liu, Y. Wang, L. Ren, Immobilization of an antimicrobial peptide on silicon surface with stable activity by click chemistry, J. Mater. Chem. B 6 (2018) 68–74, https://doi.org/10.1039/C7TB02557B.
[8] P. Rossini, L. Napolano, G. Matteucci, Biotoxicity and life cycle assessment of two commercial antifouling coatings in marine systems, Chemosphere 237 (2019) 124475, https://doi.org/10.1016/j.chemosphere.2019.124475.
[9] S. Barman, L.B. Kurnaz, R. Leighton, M.W. Hossain, A.W. Decho, C. Tang, Intrinsic antimicrobial resistance: molecular biomaterials to combat microbial biofilms and bacterial persisters, Biomaterials 311 (2024) 122690, https://doi.org/10.1016/j.biomaterials.2024.122690.
[10] T. Wei, W. Zhan, L. Cao, C. Hu, Y. Qu, Q. Yu, H. Chen, Multifunctional and regenerable antibacterial surfaces fabricated by a universal strategy, ACS Appl. Mater. Interfaces 8 (2016) 30048–30057, https://doi.org/10.1021/acsami.6b11187.
[11] X. Wang, C. Chen, J. Hu, C. Liu, Y. Ning, F. Lu, Current strategies for monitoring and controlling bacterial biofilm formation on medical surfaces, Ecotoxicol. Environ. Saf. 282 (2024) 116709, https://doi.org/10.1016/j.ecoenv.2024.116709.
[12] I. Francolini, L. Hall-Stoodley, P. Stoodley, 2.2.8 - Biofilms, Biomaterials, and Device-Related Infections, in: W.R. Wagner, S.E. Sakiyama-Elbert, G. Zhang, M. J. Yaszemski (Eds.), Biomaterials Science, (Fourth Edition), Academic Press, 2020, pp. 823–840, https://doi.org/10.1016/B978-0-12-816137-1.00054-4.
[13] X. Jin, J. Yuan, J. Shen, Zwitterionic polymer brushes *via* dopamine-initiated ATRP from PET sheets for improving hemocompatible and antifouling properties, Colloids Surf. B Biointerfaces 145 (2016) 275–284, https://doi.org/10.1016/j.colsurfb.2016.05.010.
[14] L. Mi, S. Jiang, Integrated antimicrobial and nonfouling zwitterionic polymers, Angew. Chem. Int. Ed. 53 (2014) 1746–1754, https://doi.org/10.1002/anie.201304060.
[15] J. Li, R. Ma, Z. Wu, S. He, Y. Chen, R. Bai, J. Wang, Visible-light-driven ag-modified TiO2 thin films anchored on bamboo material with antifungal memory activity against *Aspergillus niger*, J. Fungi 7 (2021) 592, https://doi.org/10.3390/jof7080592.
[16] K. Odokonyero, A. Gallo, H. Mishra, Nature-inspired wax-coated jute bags for reducing post-harvest storage losses, Sci. Rep. 11 (2021) 15354, https://doi.org/10.1038/s41598-021-93247-z.
[17] C.R. Thornton, Chapter one - detection of the 'big five' mold killers of humans: aspergillus, fusarium, lomentospora, scedosporium and mucormycetes, in: G. M. Gadd, S. Sariaslani (Eds.), Advances in Applied Microbiology, Academic Press, 2020, pp. 1–61, https://doi.org/10.1016/bs.aambs.2019.10.003.
[18] G.D. Brown, D.W. Denning, N.A.R. Gow, S.M. Levitz, M.G. Netea, T.C. White, Hidden killers: human fungal infections, Sci. Transl. Med. 4 (2012), https://doi.org/10.1126/scitranslmed.3004404, 165rv13-165rv13.
[19] Z. Xie, G. Li, X. Wang, Chiral stereochemical strategy for antimicrobial adhesion, in: B. Li, T.F. Moriarty, T. Webster, M. Xing (Eds.), Racing for the Surface, Springer International Publishing, Cham, 2020, pp. 431–456, https://doi.org/10.1007/978-3-030-34475-7_19.
[20] J. Xu, H. Zhao, Z. Xie, S. Ruppel, X. Zhou, S. Chen, J.F. Liang, X. Wang, Stereochemical strategy advances microbially antiadhesive cotton textile in safeguarding skin flora, Adv. Healthc. Mater. 8 (2019) 1900232, https://doi.org/10.1002/adhm.201900232.
[21] P. Zhang, X. Chen, F. Bu, C. Chen, L. Huang, Z. Xie, G. Li, X. Wang, Dual coordination between stereochemistry and cations endows polyethylene terephthalate fabrics with diversiform antimicrobial abilities for attack and defense, ACS Appl. Mater. Interfaces 15 (2023) 9926–9939, https://doi.org/10.1021/acsami.2c19323.
[22] Y. Xin, H. Zhao, J. Xu, Z. Xie, G. Li, Z. Gan, X. Wang, Borneol-modified chitosan: antimicrobial adhesion properties and application in skin flora protection, Carbohydr. Polym. 228 (2020) 115378, https://doi.org/10.1016/j.carbpol.2019.115378.
[23] E.P. Magennis, A.L. Hook, P. Williams, M.R. Alexander, Making silicone rubber highly resistant to bacterial attachment using thiol-ene grafting, ACS Appl. Mater. Interfaces 8 (2016) 30780–30787, https://doi.org/10.1021/acsami.6b10986.
[24] Q. Zhang, Y. Yang, D. Suo, S. Zhao, J.C.-W. Cheung, P.H.-M. Leung, X. Zhao, A biomimetic adhesive and robust janus patch with anti-oxidative, anti-inflammatory, and anti-bacterial activities for tendon repair, ACS Nano 17 (2023) 16798–16816, https://doi.org/10.1021/acsnano.3c03556.
[25] X. Ruan, X. Deng, M. Tan, C. Yu, M. Zhang, Y. Sun, N. Jiang, In vitro antibiofilm activity of resveratrol against avian pathogenic *Escherichia coli*, BMC Vet. Res 17 (2021) 249, https://doi.org/10.1186/s12917-021-02961-3.
[26] X. Hu, Y. Zhang, Z. Chen, Y. Gao, B. Teppen, S.A. Boyd, W. Zhang, J.M. Tiedje, H. Li, Tetracycline accumulation in biofilms enhances the selection pressure on *Escherichia coli* for expression of antibiotic resistance, Sci. Total Environ. 857 (2023) 159441, https://doi.org/10.1016/j.scitotenv.2022.159441.
[27] W. Feng, M. Chittò, W. Xie, Q. Ren, F. Liu, X. Kang, D. Zhao, G. Li, T.F. Moriarty, X. Wang, Poly(d -amino acid) nanoparticles target *Staphylococcal* growth and biofilm disassembly by interfering with peptidoglycan synthesis, ACS Nano 18 (2024) 8017–8028, https://doi.org/10.1021/acsnano.3c10983.
[28] X. Kang, X. Yang, F. Bu, W. Feng, F. Liu, W. Xie, G. Li, X. Wang, GSH/pH cascade-responsive nanoparticles eliminate methicillin-resistant *Staphylococcus aureus* biofilm via synergistic photo-chemo therapy, ACS Appl. Mater. Interfaces 16 (2024) 3202–3214, https://doi.org/10.1021/acsami.3c17198.
[29] J. Xu, Z. Xie, F. Du, X. Wang, One-step anti-superbug finishing of cotton textiles with dopamine-menthol, J. Mater. Sci. Technol. 69 (2021) 79–88, https://doi.org/10.1016/j.jmst.2020.08.007.
[30] E. Melloul, L. Roisin, M.-F. Durieux, P.-L. Woerther, D. Jenot, V. Risco, J. Guillot, E. Dannaoui, J.-W. Decousser, F. Botterel, Interactions of Aspergillus fumigatus and Stenotrophomonas maltophilia in an in vitro mixed biofilm model: does the strain matter? Front. Microbiol. 9 (2018) https://doi.org/10.3389/fmicb.2018.02850.
[31] W. Sun, Y. Yu, J. Chen, B. Yu, T. Chen, H. Ying, S. Zhou, P. Ouyang, D. Liu, Y. Chen, Light signaling regulates Aspergillus niger biofilm formation by affecting melanin and extracellular polysaccharide biosynthesis, mBio 12 (2021), https://doi.org/10.1128/mbio.03434-20.
[32] L. Liu, B. Yu, W. Sun, C. Liang, H. Ying, S. Zhou, H. Niu, Y. Wang, D. Liu, Y. Chen, Calcineurin signaling pathway influences *Aspergillus niger* biofilm formation by affecting hydrophobicity and cell wall integrity, Biotechnol. Biofuels 13 (2020) 54, https://doi.org/10.1186/s13068-020-01692-1.
[33] Z. Xie, C. Chen, X. Chen, F. Bu, G. Li, P. Zhang, X. Wang, In situ borneol-modified polyester with antibacterial adhesion and long-term fungal-repellent properties, React. Funct. Polym. 202 (2024) 105993, https://doi.org/10.1016/j.reactfunctpolym.2024.105993.
[34] Z. Xiu, M. Yang, R. Wu, C. Lei, H.-M. Ren, B. Yu, S. Gao, S. Duan, D. Wu, F.-J. Xu, Scalable anti-infection polyurethane catheters with long-acting and autoclavable properties, Chem. Eng. J. 451 (2023) 138495, https://doi.org/10.1016/j.cej.2022.138495.
[35] X. Li, X. Wang, S. Subramaniyan, Y. Liu, J. Rao, B. Zhang, Hyperbranched polyesters based on indole- and lignin-derived monomeric aromatic aldehydes as effective nonionic antimicrobial coatings with excellent biocompatibility, Biomacromolecules 23 (2022) 150–162, https://doi.org/10.1021/acs.biomac.1c01186.
[36] F. Du, W. A, F. Liu, B. Wu, Y. Liu, W. Zheng, W. Feng, G. Li, X. Wang, Hydrophilic chitosan/graphene oxide composite sponge for rapid hemostasis and non-rebleeding removal, Carbohydr. Polym. 316 (2023) 121058, https://doi.org/10.1016/j.carbpol.2023.121058.
[37] D. Tahk, S. Bang, S. Hyung, J. Lim, J. Yu, J. Kim, N.Li Jeon, H.Nam Kim, Self-detachable UV-curable polymers for open-access microfluidic platforms, Lab a Chip 20 (2020) 4215–4224, https://doi.org/10.1039/D0LC00604A.
[38] X. Liu, S. Liu, Y. Fan, J. Qi, X. Wang, W. Bai, D. Chen, C. Xiong, L. Zhang, Biodegradable cross-linked poly(L-lactide-co-ε-caprolactone) networks for ureteral

stent formed by gamma irradiation under vacuum, J. Ind. Eng. Chem. 104 (2021) 73–84, https://doi.org/10.1016/j.jiec.2021.08.014.
[39] S. Li, Z. Guo, H. Zhang, X. Li, W. Li, P. Liu, Y. Ren, X. Li, ABC triblock copolymers antibacterial materials consisting of fluoropolymer and polyethylene glycol antifouling block and quaternary ammonium salt sterilization block, ACS Appl. Bio Mater. 4 (2021) 3166–3177, https://doi.org/10.1021/acsabm.0c01571.
[40] P. Kaner, E. Rubakh, D.H. Kim, A. Asatekin, Zwitterion-containing polymer additives for fouling resistant ultrafiltration membranes, J. Membr. Sci. 533 (2017) 141–159, https://doi.org/10.1016/j.memsci.2017.03.034.
[41] Q. Duan, Y. Wang, S. Chen, M. Miao, S. Chen, D. Zhang, Functionalized carbon nanotube films by thiol-ene click reaction, Appl. Surf. Sci. 486 (2019) 144–152, https://doi.org/10.1016/j.apsusc.2019.05.011.
[42] W. Huang, Y. Li, M. Chen, J. Chen, J. Liu, S. Xiang, F. Fu, X. Liu, N. Li, Durable antibacterial cotton fiber surface fabricated by the thiol-ene click reaction between eugenol and L-cysteine, Appl. Surf. Sci. 643 (2024) 158742, https://doi.org/10.1016/j.apsusc.2023.158742.
[43] Y. Yuan, Y. Shang, Y. Zhou, J. Guo, F. Yan, Enabling antibacterial and antifouling coating via grafting of a nitric oxide-releasing ionic liquid on silicone rubber, Biomacromolecules 23 (2022) 2329–2341, https://doi.org/10.1021/acs.biomac.2c00077.
[44] H. Liu, M. Liu, B. Zheng, J. Han, F. Fan, A preliminary study of the temperature-responsive selective extraction performance of hydrogel derived from sulfobetaine methacrylate, Anal. Chim. Acta 1319 (2024) 342958, https://doi.org/10.1016/j.aca.2024.342958.
[45] C. Liu, F. Cheng, B. Liu, D. Gao, G. Cheng, C. Li, H. Wang, W. He, Versatile, oxygen-insensitive surface-initiated anionic polymerization to prepare functional polymer brushes in aqueous solutions, Langmuir 38 (2022) 1001–1010, https://doi.org/10.1021/acs.langmuir.1c02416.
[46] J. Wu, C. He, H. He, C. Cheng, J. Zhu, Z. Xiao, H. Zhang, X. Li, J. Zheng, J. Xiao, Importance of zwitterionic incorporation into polymethacrylate-based hydrogels for simultaneously improving optical transparency, oxygen permeability, and antifouling properties, J. Mater. Chem. B 5 (2017) 4595–4606, https://doi.org/10.1039/C7TB00757D.
[47] Q. Liu, J. Locklin, Transparent grafted zwitterionic copolymer coatings that exhibit both antifogging and self-cleaning properties, ACS Omega 3 (2018) 17743–17750, https://doi.org/10.1021/acsomega.8b02867.
[48] S. Wu, K. Yan, B. He, Y. Wang, S. Xue, S. Liu, Q. Ye, F. Zhou, Preparation of tannic acid based zwitterionic polymer functionalized coating on glass surface for antibacterial and antifouling applications, Prog. Org. Coat. 194 (2024) 108578, https://doi.org/10.1016/j.porgcoat.2024.108578.
[49] L. Cheng, C. Liu, J. Wang, Y. Wang, W. Zha, X. Li, Tough hydrogel coating on silicone rubber with improved antifouling and antibacterial properties, ACS Appl. Polym. Mater. 4 (2022) 3462–3472, https://doi.org/10.1021/acsapm.2c00069.